Carbohydrate Polymers 84 (2011) 524–532

Contents lists available at ScienceDirect

Carbohydrate Polymers

journal homepage: www.elsevier.com/locate/carbpol

On the external morphology of native cellulose microfibrils

Karim Mazeau [1]

Centre de Recherches sur les Macromolécules Végétales (CERMAV-CNRS), BP53, 38041 Grenoble cedex 9, France

ARTICLE INFO

Article history:
Received 2 June 2010
Accepted 6 December 2010
Available online 13 December 2010

Keywords:
Cellulose
External morphology
Surface
Exposure
Roughness
Surface energy

ABSTRACT

This study is based on the working hypothesis that the external morphology of the cellulose microfibrils is correctly represented by a combination of eight surfaces issued from four lateral cleavage planes of the I-α and I-β allomorphs. Models of these surfaces have been generated and investigated before and after relaxation, thus allowing one to predict, for each of these, their roughness, the accessibility of the hydrophilic and hydrophobic groups as well as their surface and attachment energies. Results showed that the ensemble of eight surfaces could be divided into three families. The first family contains four hydrophilic and moderately rough surfaces, which dominate the external morphology of the microfibrils and are thus responsible for their macroscopic properties. Surfaces of the two other families are of minor importance in the external morphology as they are located at the corners of the cellulosic macrocrystals. They are either flat and hydrophobic or rough and hydrophilic. The flat surfaces are of high biological and technical significance as they are specifically recognized by hydrophobic substances, including the cellulose binding modules of cellulases. Relaxation resulted in a significant disorganization of the rough surfaces whereas the other surfaces remain close to their original organisation. The interpretation of the surface and attachment energies of the surfaces, evidences the major influence of the biosynthetic process in the design of the external morphology of the cellulose microfibrils, as opposed to the classical kinetic and thermodynamic crystal growth mechanism.

1. Introduction

Many of the functional properties of cellulose depend on its capacity to interact with diverse entities, ranging from small molecules to elaborate macromolecules, possessing various polarities. Example of this diversity is illustrated with the adsorption of hydrophilic hemicelluloses on cellulose microfibrils, a critical step for the development of lignin within maturing wood cells (Carpita & Gibeaut, 1993). In another documented case, it is the specific adsorption of the hydrophobic cellulose-binding module (CBM) of cellulases that enhances the biodegradation yield of cellulosic biomass (Himmel et al., 2007). Thus, the surface characteristics of cellulose present multiple facets and it is important to know their details if one want to find new end uses for cellulose. For instance, in the evolving field of cellulose-based nanocomposites, it is clear that the mechanical properties of these new materials will be optimized if the chosen matrix is well adapted for a strong compatibility with the cellulose surfaces.

With cellulose, the adsorption and adhesion phenomena depend on the organization of the glucan chains located at the surface of the cellulose microfibrils. The crystalline core of these microfibrils has been extensively studied (Nishiyama, 2009): it consists of slender crystalline phases made of two allomorphs, namely the one chain triclinic I-α and the two chain monoclinic phase I-β. The long crystals are regularly interrupted by short amorphous zones: for instance, in ramie cellulose, the crystals are about 300 glucosyl units long, whereas only 4–5 units occur in the amorphous regions (Nishiyama, Kim, et al., 2003). Much less is known about the surface of the cellulose microfibrils. Given the 2_1 helical conformation adopted by the cellulose molecules together with the equatorial orientation of the hydroxyl groups, one may anticipate that the cellulose microfibrils expose a variety of surfaces possessing a spectrum of characteristics. Inverse gas chromatography experiments give an average surface energy of 50–70 mJ m^{-2} (Aulin et al., 2009; Erbil, 1996; Forsstroem, Eriksson, & Waagberg, 2005; Mills, Gardner, & Wimmer, 2008; Swaminathan, Cobb, & Saracovan, 2006; Trejo-O'Reilly, Cavaille, Belgacem, & Gandini, 1998). This value, which is often used for estimating the compatibility of cellulose with potentially adsorbable molecular species, fails to reflect the diversity of the values that are present when going from one surface to the other.

The ultrastructural description of the surface of the cellulose microfibrils relies on specific microscopy techniques. Transmission electron microscopy, operated either in microdiffraction or in diffraction contrast modes, can reveal the cross-section of large crystalline microfibrils such as those of *Valonia*, *Micrasterias* or tunicin and identify their surfaces (Daele, Revol, Gaill, & Goffinet,

E-mail address: karim.mazeau@cermav.cnrs.fr
[1] Affiliated with Joseph Fourier University, and member of the Institute of Molecular Chemistry of Grenoble.

0144-8617/$ – see front matter © 2010 Elsevier Ltd. All rights reserved.
doi:10.1016/j.carbpol.2010.12.016

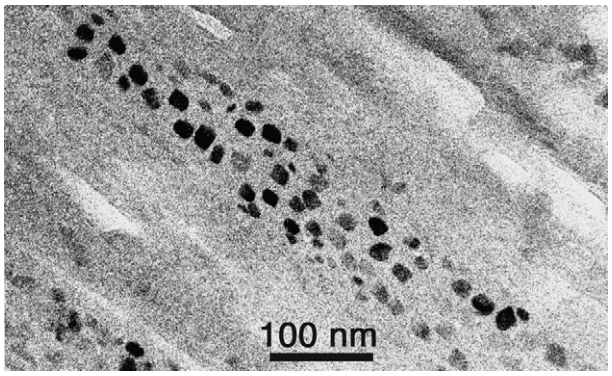

Fig. 1. Diffraction contrast electron micrograph image of *Valonia ventricosa* cell wall section with the microfibrillar orientation perpendicular to the plane of observation. Each microfibril is seen as a black squarish section, with sides of the order of 20 nm, corresponding to the (0 1 0) and (1 0 0) planes in the cellulose I-α system. The microfibrils are organized in crisscrossed layers with surface along the (1 0 0) plane in the I-α allomorph definition and (1 −1 0) in the I-β definition.

1992; Hanley, Giasson, Revol, & Gray, 1992; Helbert, Nishiyama, Okano, & Sugiyama, 1998; Helbert, Sugiyama, Kimura, & Itoh, 1998; Kim, Herth, Vuong, & Chanzy, 1996; Revol, 1982; Sassi & Chanzy, 1995; Sassi, Tekely, & Chanzy, 2000; Sugiyama, Harada, Fujiyoshi, & Uyeda, 1985). In *Valonia*, which has been the most studied, the microfibril sections are squarish (Fig. 1), with four developed surfaces defined by the hydrophilic (1 1 0) and (1 −1 0) planes for the I-β allomorph and/or the (1 0 0) and (0 1 0) planes for the I-α phase, according to the unit cell definitions of Sugiyama, Vuong, and Chanzy (1991). As observed by several authors and illustrated in Fig. 1, the corner of the crystals are frequently blunt, and thus secondary surfaces, corresponding to other planes are also present. The minor (1 −1 0) surface of the I-α phase of *Valonia* is one of them. This hydrophobic surface is quite important since it was proven to be the binding site for the CBM of the Cel7A cellulase from *Trichoderma reesei* (Lehtio et al., 2003; Xu et al., 2009), the first step leading to the digestion of crystalline cellulose by this effective enzyme.

High resolution AFM should be the technique of choice to describe the molecular details of the surfaces of cellulose. Due to experimental difficulties, only few high-resolution AFM images have been published so far, describing only the (1 0 0) triclinic surface of *Valonia* microfibrils (Baker, Helbert, Sugiyama, & Miles, 1998, 2000). In these images, a regular organization of the glucan chains is perceptible, indicating a *gt* conformation of the exposed hydroxymethyl groups, different from the *tg* situation of these groups within the core of the crystal. This interpretation is partly supported by either molecular dynamics (Bergenstrahle, Wohlert, Larsson Per, Mazeau, & Berglund Lars, 2008; Heiner & Teleman, 1997; Heiner, Kuutti, & Teleman, 1998) or by solid-state ^{13}C NMR measurements (Newman & Davidson, 2004), which clearly indicate a mixture of *gg* and *tg* conformations, together with some disorganization of the surface hydroxymethyl groups.

Taken together the aforementioned experimental descriptions of the cellulose surface are limited and the properties of most of the native cellulose surfaces exposed to the external environment remain to be ascertained. Molecular modelling can be used in this context to complement the paucity of experimental data. We have recently created molecular models of one amorphous and four organized cellulose surfaces from the I-β crystal, namely the (1 1 0), (1 −1 0), (0 1 0) and (1 0 0) (Da Silva Perez, Ruggiero, Morais, Machado, & Mazeau, 2004; Mazeau & Vergelati, 2002). These models were used to characterize some of the surface properties of native cellulose microfibrils. Remarkably, the dynamics of the surface chains of the (1 1 0) and (1 −1 0) surfaces differed significantly (Bergenstrahle, Wohlert, et al., 2008), and the contact angle of a water drop on the (1 1 0) and (1 0 0) surfaces was also substantially different (Mazeau & Rivet, 2008). These models have proven useful to predict the adhesion of synthetic polymers on cellulose by either selecting suitable polymers (Chauve, Heux, Arouini, & Mazeau, 2005) or modifying the surface of cellulose (Bergenstrahle, Mazeau, & Berglund, 2008) to accommodate them.

The modelling reports have so far been only fragmentary, with the consequence that many features of the potential cellulose crystalline surfaces are still lacking. The goal of the present paper is therefore to model in a comprehensive way the basic cleavage surfaces of native cellulose crystals. Eight surfaces of lowest Miller indices: four surfaces for each of the I-α and the I-β phases were selected as being the most probable in terms of crystal growth theory (Donnay & Harkei, 1937). For each individual surface, this paper focuses on the prediction of the roughness, the accessibility of the hydrophobic and hydrophilic groups, together with surface and attachment energies.

2. Experimental

The calculations were done with the *Cerius*^{2} molecular modelling package (Accelrys Inc.), at the Centre d'Expérimentation et de Calcul Intensif (CECIC), Grenoble, France.

2.1. Models

Graphical illustrations of the surfaces and the procedure used for their building are presented in Figs. 2 and 3, showing the definitions of the cleavage planes in the I-α and I-β crystalline systems (Fig. 2) and the build up of the models in the case of cellulose I-β (Fig. 3).

Coordinates, taken from the CIF files of the I-α (Nishiyama, Sugiyama, Chanzy, & Langan, 2003) and I-β (Nishiyama, Langan, & Chanzy, 2002) crystal structures, were used in this study. The I-α lattice parameters were first redefined in order to have the *c* axis of the unit cell coincident with the chain axis. Four infinite bulk models were built: two for the I-α phase and two for the I-β phase. Their surfaces are defined according to their Miller indices followed by a Greek letter, which refers to the considered allomorph: for example, the surface (1 1 0) of the I-β allomorph is indicated as (1 1 0)β, etc. In the case of cellulose I-β, they had the crystallographic planes (1 0 0) and (0 1 0) or (1 1 0) and (1–10) parallel to the *ac* and *bc* planes of the parent unit cell (Fig. 3). In the models, each individual cellulose chain was defined with eight independent residues. These four models were then duplicated to obtain the super cells P1, defined along *a*′, *b*′ and *c*′ parameters. Covalent bonds between one end of the mother chain and the other end of the image chain across the periodic box were created to model infinite chains of cellulose. The P1 cells were then relaxed by molecular dynamics in the NPT ensemble according to the protocol described elsewhere (Mazeau, 2005; Mazeau & Heux, 2003).

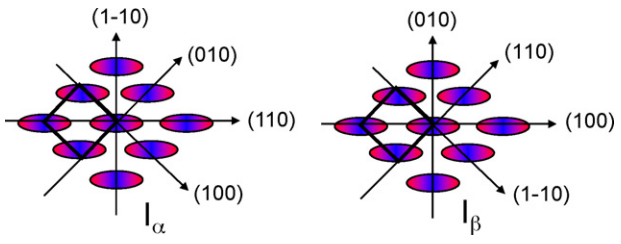

Fig. 2. Schematic representation of glucan chains in a crystalline organization representing the two native allomorphs of cellulose projected perpendicular to the chain axis. The arrows indicate the cleavage planes together with the Miller indices of the corresponding surfaces.

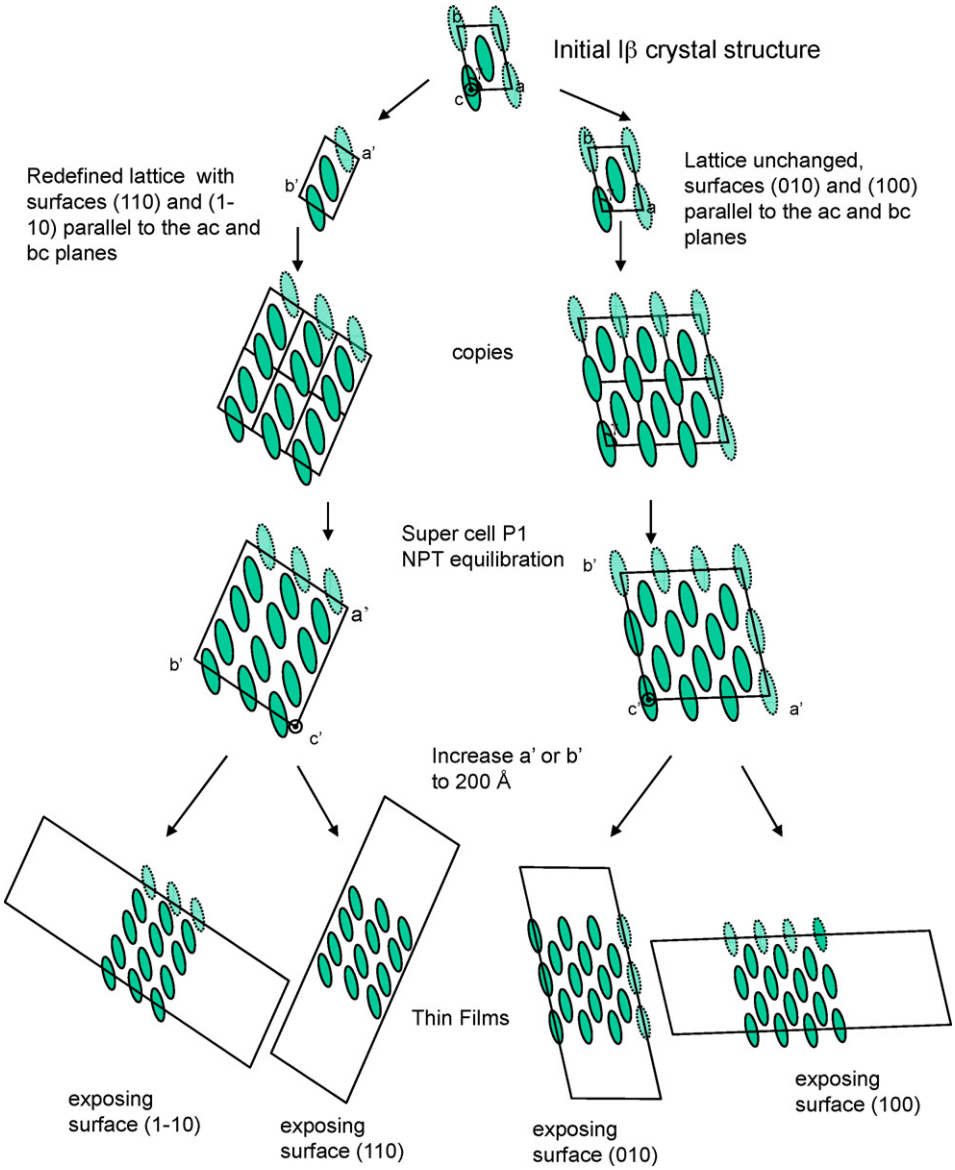

Fig. 3. Schematic description of the modelling procedure to create cellulose surfaces from the crystalline bulks. The case of cellulose I-β is illustrated in this case. Molecular models of the four surfaces are shown in Fig. 4.

The parameters a' or b' were then increased to 200 Å to create thin films of cellulose (Fig. 4), exposing two equivalent surfaces. Since the super-cells were subjected to periodic boundary conditions, the resulting surfaces were then infinite. The 200 Å distance was large enough to provide a sufficient free volume above the bulk of cellulose and thus to avoid interactions between the two cellulose surfaces of a given cell. The cell dimensions of the final systems together with the number of chains, surface chains and layers are given in Table 1.

2.2. Surface relaxation

Solid state NMR spectroscopy (Newman & Davidson, 2004; Vietor, Newman, Ha, Apperley, & Jarvis, 2002), together with previous modelling (Bergenstrahle, Wohlert, et al., 2008; Heiner & Teleman, 1997; Heiner et al., 1998) have indicated that since only the surface chains were affected by the interface, they were then less organized than the interior chains. To save computational time, the most inner layers of chains were constrained in our models. The

Table 1
Characteristics of the final models. Each individual cellulose chain possesses eight residues.

Allomorph	Miller indices	a' (Å)	b' (Å)	c' (Å)	α (°)	β (°)	γ (°)	Model thickness (Å)	N chains/surf	N layers
I-α	(0 1 0)	200	53.37	42.73	111.65	63.61	96.28	47.99	8	8
	(1 0 0)	47.99	200	42.73	111.65	63.61	96.28	53.37	8	8
	(1 −1 0)	200	56.73	42.74	122.83	88.66	83.92	50.81	12	6
	(1 1 0)	50.81	200	42.74	122.83	88.66	83.92	56.73	6	12
I-β	(1 1 0)	200	46.06	41.85	89.98	90.10	81.90	43.29	8	8
	(1 −1 0)	43.29	200	41.85	89.98	90.10	81.90	46.06	8	8
	(1 0 0)	200	50.64	41.86	90.00	90.00	93.5	43.97	6	12
	(0 1 0)	43.97	200	41.86	90.00	90.00	93.5	50.64	12	6

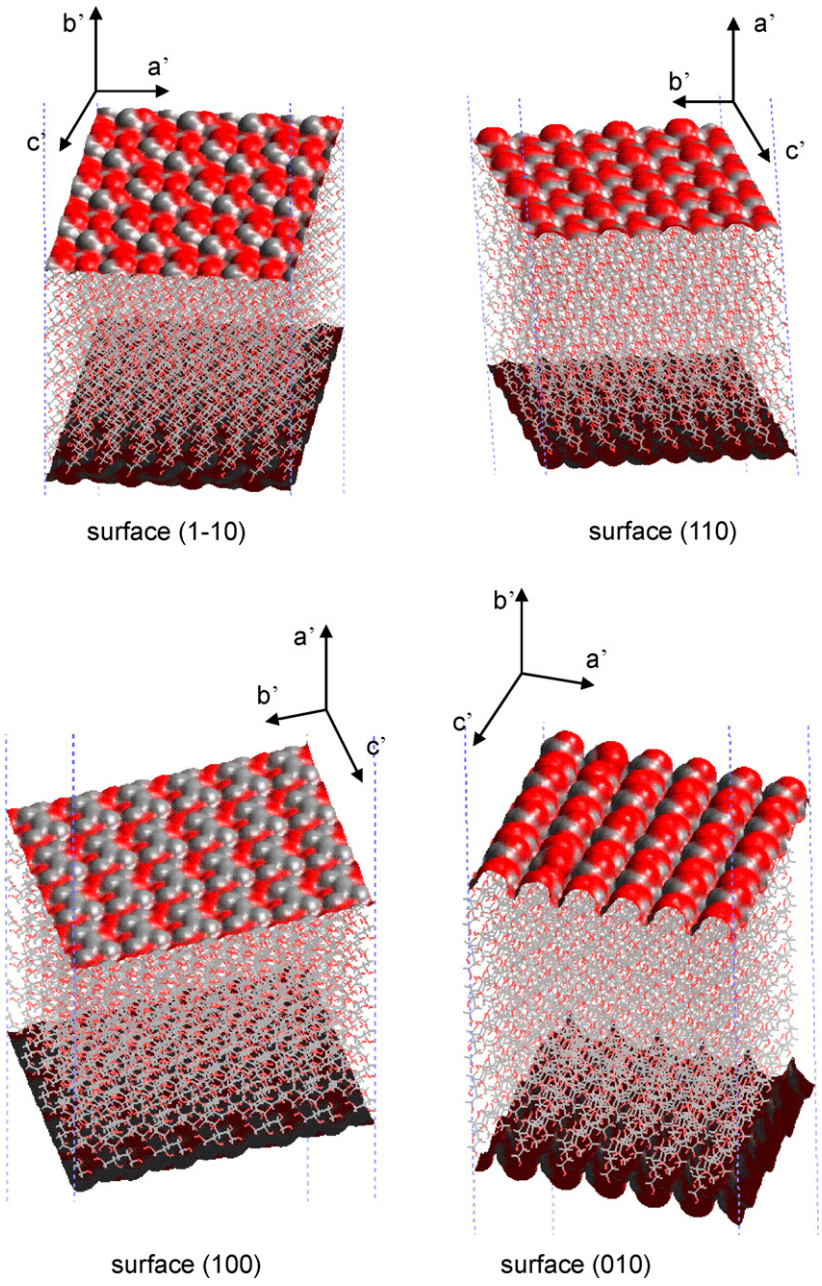

Fig. 4. Molecular models of the four surfaces of the I-β allomorph. In each case, *c'* is the chain axis.

relaxation of the models was performed by minimization and by a simulated annealing procedure that consisted of 100 ps molecular dynamic (MD) in the NVT ensemble at 400 K followed by 400 ps MD at 300 K and further minimization.

2.3. Computational procedure

The pcff-300-1.01 (Sun, Mumby, Maple, & Hagler, 1994) second generation force-field was employed. A brief description of the analytical form of the potential energy function can be found elsewhere (Mazeau & Heux, 2003). The charge equilibration method was used to calculate the point charges for each atom (Rappe & Goddard, 1991). The cut-in and cut-off distances were fixed at 10 Å and 11 Å, respectively. The minimum image convention was imposed in order not to duplicate non-bonded calculations. The minimization uses the conjugate gradient procedure with, as convergence criterion, the root–mean–square of the atomic derivatives taken as 0.05 kcal/(mol Å). The equations of motion in the molecular dynamics procedure were solved using the Verlet algorithm (Verlet, 1967), with a time step of 1 fs. The system is coupled to a bath at $T = 300$ K using the Nose's algorithm (Nose, 1984a, 1984b).

3. Results

3.1. Characteristics of the relaxed surfaces

3.1.1. Surface deformation

A comparison between the initial and relaxed structures allows one to evaluate the amount of deformation experienced by the surface chains during the relaxation process. A global value of this deformation is quantified by the root mean square deviation (RMSD) of the coordinates of the carbon and oxygen atoms. Fig. 5 presents the RMSD data for the eight surfaces that are considered. Six of them display a small RMSD whereas two surfaces, namely

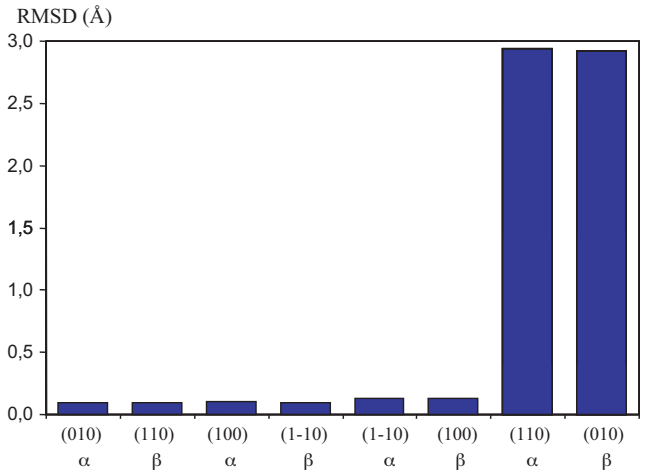

Fig. 5. Root mean square deviation (RMSD) of the coordinates of the carbon and oxygen atoms of the surface chains during the relaxation process for the eight different surfaces.

the (0 1 0)β and (1 −1 0)α become reorganized strongly during molecular dynamics. The deformations result not only from global translation and rotation of the surface chains, but also from their conformational reorganization. Example of such extensive reorganization can be visualized in the molecular model showing the (0 1 0)β surface (Fig. 6).

3.1.2. Surface roughness

The surface roughness is another important parameter of the surface micro texture. Among the standards that describe the surface roughness, we have chosen the average roughness parameter *R*, which is determined as follows:

$$R = \sqrt{\frac{\sum_{n=1}^{N}(Zn - \langle Z\rangle)^2}{N-1}} \quad (1)$$

where *Zn* represents the height of the *n*th coordinate, ⟨*Z*⟩ is equal to the mean height of *Zn* and *N* is the number of coordinates.

The values of *R* roughness of the relaxed surfaces are given in Fig. 7, which clearly shows that the surface micro-texture depends on the cleavage plane of the cellulose crystal, with *R* values ranging from 0.67 Å to 1.57 Å. Following these measurements the crystal surfaces can be divided into three families, namely the flat (1 0 0)β and (1 −1 0)α, the moderately rough (0 1 0)α, (1 1 0)β, (1 0 0)α and the (1 −1 0)β and the very rough ones (1 1 0)α and (0 1 0)β. Remarkably, the observed differences between equivalent surfaces from the I-α and I-β allomorphs are not significant.

3.1.3. Surface accessibility

This important parameter describes the accessibility of the functional atoms and moieties such the acetals and the hydroxyls, together with the hydrophobic CH groups. The accessibility can be calculated from the ratio between the Connolly surface of given atoms or moieties and that of the total Connolly surface, using for the calculation a probe radius of 1.4 Å, which corresponds to the size of a water molecule.

The accessibility of each of the hydrophilic groups and atoms are given in Table 2, whereas those of the sum of all the hydrophilic groups, namely the hydroxyls and acetal oxygens, are reported in Fig. 8. Taken together, the results presented in Table 2 and Fig. 8, indicate that differences in accessibility of the eight surfaces are globally small. Quite remarkably the ratio between the hydrophobic and hydrophilic domains is systematically close to unity, indicating that both characters are significantly present in all surfaces, which therefore present amphiphilic properties.

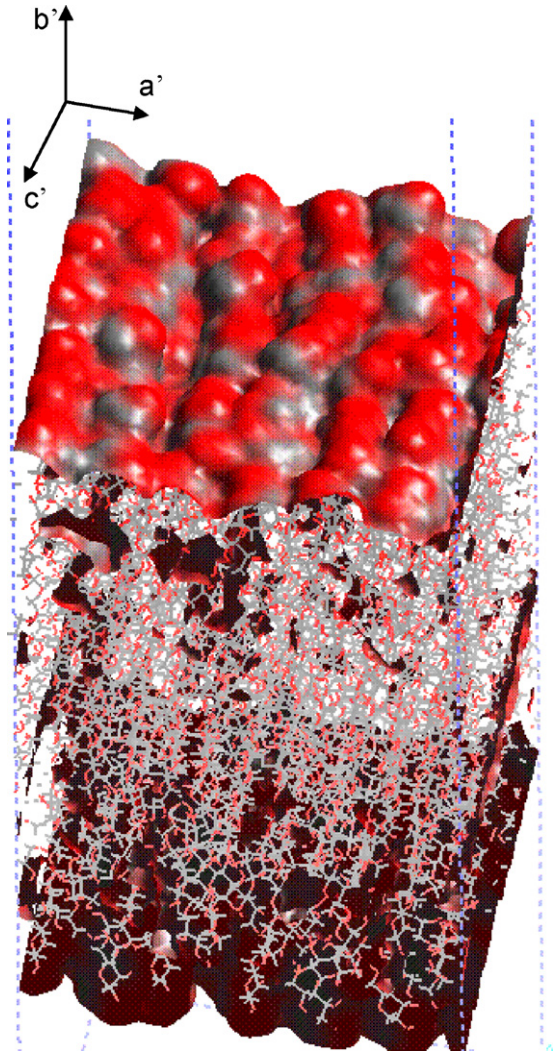

Fig. 6. Molecular model of the relaxed (0 1 0)β surface. This relaxed model has to be compared with the initial model shown in Fig. 4; *c*′ is along the cellulose chain axis.

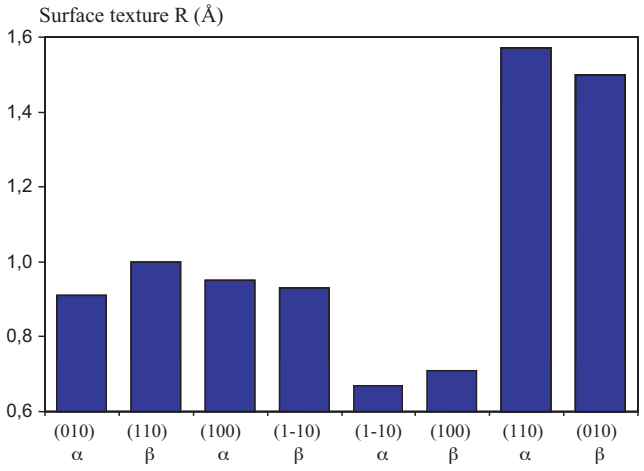

Fig. 7. Roughness of the eight different surfaces.

Table 2
Accessibility (%) of selected atoms and groups.

Allomorph	Plane	O6H	O2H	O3H	ΣOH	O5	O4	ΣO acetals	C–H
I-α	(0 1 0)	13.41	11.33	12.77	37.51	6.08	7.08	13.16	49.34
	(1 0 0)	13.98	12.50	11.81	38.29	5.40	5.52	10.92	50.79
	(1 –1 0)	14.60	14.07	13.90	42.57	6.55	5.60	12.15	45.28
	(1 1 0)	7.70	6.60	8.99	23.29	10.03	6.29	16.32	60.39
I-β	(1 1 0)	13.20	11.81	12.94	37.95	4.75	7.22	11.97	50.07
	(1 –1 0)	12.43	12.95	13.37	38.75	6.34	4.34	10.68	50.57
	(1 0 0)	8.70	8.50	8.28	25.48	9.76	7.80	17.56	56.96
	(0 1 0)	13.90	13.21	14.20	41.31	6.94	5.94	12.88	45.81

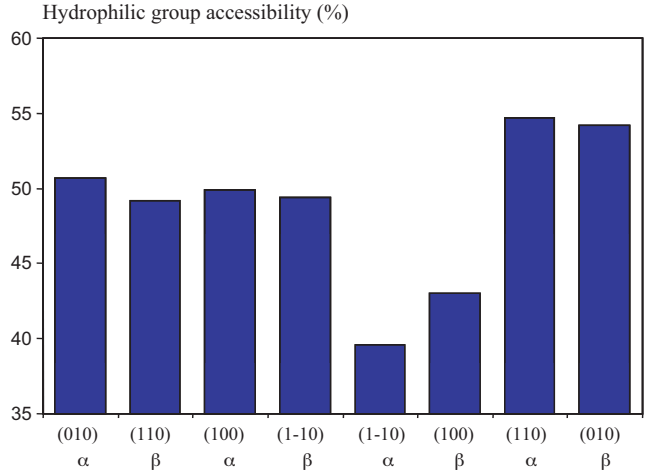

Fig. 8. Accessibility of the hydrophilic groups (%) of the eight different surfaces.

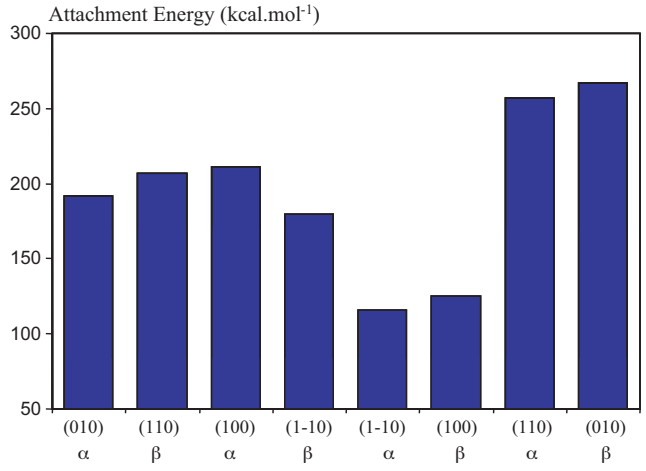

Fig. 10. Attachment energies of the eight different surfaces.

3.2. Energies

3.2.1. Surface energy

The surface energy (γ) is the energy required to cleave the crystal in order to expose the surface; it is calculated according to:

$$\gamma = \frac{(E_{surf} - E_{bulk})}{2A}$$

where E_{surf} is the energy of the unrelaxed surface, whereas E_{bulk} is the energy of the bulk and A is the surface area.

Predicted surface energies of the 8 surfaces are given in Fig. 9, which indicates values ranging from 150 to 350 mJ m^{-2}. These values are considerably larger than 50 mJ m^{-2} obtained experimentally either by gas chromatography or contact angles data measurements, using drops of liquids of different polarities (Gandini & Belgacem, 2005; Trejo-O'Reilly et al., 1998).

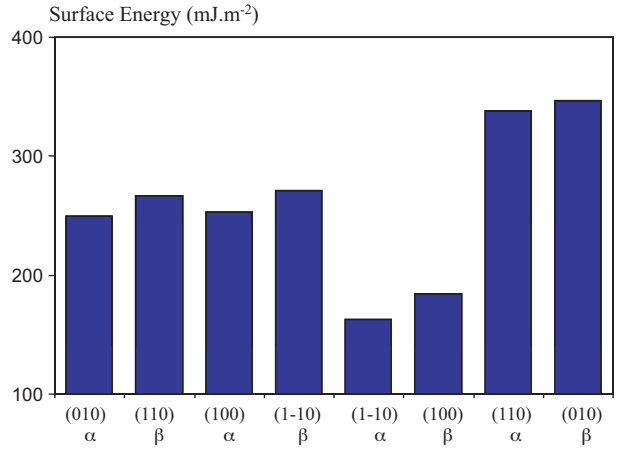

Fig. 9. Surface energies of the eight different surfaces.

3.2.2. Attachment energy

The attachment energy (E_{attach}) is the energy released when a new layer of molecules is deposited onto the surface of the crystal. It is calculated according to:

$$E_{attach} = E_{crystal} - E_{laver}$$

where $E_{crystal}$ is the energy of the crystal, E_{layer} is the energy of a layer of molecules and E_{attach} is the interaction energy between the newly added layer and the rest of the crystal.

Attachment energies, which are reported in Fig. 10, reflect the cohesion energy of a surface layer of cellulose with the rest of the crystal. The most cohesive surfaces, the (1 1 0)α and (0 1 0)β surfaces, are those, which logically have the largest surface per residue in contact.

4. Discussion

The results presented in this study give valuable insights on the surface properties of cellulose crystals, both for the crystals of the I-α and the I-β phases. In this work, we have considered not only the hydrophilic surfaces of cellulose, namely the (1 1 0)β and (1 –1 0)β, the (1 0 0)α and (0 1 0)α, the (1 –1 0)α and (0 1 0)β, but also the hydrophobic surfaces: the (1 0 0)β and (1 1 0)α. Whereas extensive literature details exist on the description of the (1 1 0)β and (1 –1 0)β, the (1 0 0)α and (0 1 0)α surfaces (Bergenstrahle, Mazeau, et al., 2008; Bergenstrahle, Wohlert, et al., 2008; Biermann, Hadicke, Koltzenburg, & Muller-Plathe, 2001; Da Silva Perez et al., 2004; Mazeau & Rivet, 2008; Mazeau & Vergelati, 2002), little information is given on the hydrophobic (1 1 0)α and (1 0 0)β surfaces (Besombes & Mazeau, 2005a, 2005b; Da Silva Perez et al., 2004; Hanus & Mazeau, 2006; Mazeau & Rivet, 2008) and nearly none on

the hydrophilic (1 −1 0)α and (0 1 0)β (Besombes & Mazeau, 2005a, 2005b; Da Silva Perez et al., 2004; Mazeau & Vergelati, 2002).

After examining the details of the various surfaces, it is clear, as aforementioned, that the ensemble of surfaces could be divided into three families and that the surfaces that are equivalent in the I-α and I-β systems – for instance the (1 1 0)β and the (0 1 0)α, etc. – present essentially the same characteristics. Thus all reasoning for a given allomorph system will also be good for the equivalent in the other and thus, only the features of the surfaces of the I-β form will be discussed. We have selected the I-β phase rather than the Iα because the I-β is dominant in the whole native cellulose world.

When examining the results illustrated in Figs. 5–7, one is struck by the deformational ability of the (0 1 0)β surface, which can be qualified of extreme, when compared with that of the other surfaces. The roughness of this surface is from two to three times higher than any of the other considered surfaces. This surface is covered by hydroxymethyl groups that have an important conformational mobility, denoted by low energy barriers between the three stable conformations *tg*, *gt* and *gg* (Tvaroska & Carver, 1997). The relaxation process results in an extensive reorganization of the surface chains in order to increase the number of contacts between the cellulose chains. This reshuffling is well illustrated, when comparing the initial (0 1 0)β, seen in Fig. 4, and its relaxed state in Fig. 6, where most of the regular features of the initial surface are completely lost.

As opposed to the (0 1 0)β surface, the hydrophobic (1 0 0)β is smooth. This surface is covered by an extensive layer of CH moieties attached directly to the glucosyl rings constituting the surface backbone. The net result is that the surface energy of this surface is the lowest, and the attachment energy, which is essentially of the Van-der-Waals type, is less favorable than that of the other surfaces where extensive hydrogen bonding could take place. In this surface, the cellulose chains, which are tightly bound by hydrogen bonds, are less prone to be mobile and then experience only a weak reorganization upon relaxation.

The surfaces (1 1 0)β and (1 −1 0)β are considered to be the dominant exposed surfaces of crystalline cellulose. They can be clearly identified in large cellulose microfibrils such as those of *Valonia* (see Fig. 1) (Daele et al., 1992; Hanley et al., 1992; Helbert, Nishiyama, et al., 1998; Helbert, Sugiyama, et al., 1998; Revol, 1982; Sassi & Chanzy, 1995; Sassi et al., 2000; Sugiyama et al., 1985). These two surfaces remained almost unchanged when relaxed. In addition, they have nearly the same characteristics: they significantly expose hydroxymethyl groups and present a moderate roughness, higher than that of the hydrophobic surface, but far lower than that of the (0 1 0)β.

The results shown in Table 2 and Fig. 8 describing the accessibility of the hydrophilic groups on the relaxed surfaces are interesting since they show that even with the hydrophobic (1 0 0)β, there is a residual amount of hydrophilic character that is present at the relaxed surface. Conversely, at the surfaces that are quoted hydrophilic, half of them is still covered by C–H groups. Thus, each surface can be characterized as being amphiphilic, with more or less hydrophylic or hydrophobic properties. This ubiquitous character of cellulose has always to be accounted for, when studying interactions of cellulose with chemical or biochemical reagents.

It is interesting to compare the calculated values that are reported here for the surface energy of the various surfaces with those measured experimentally, ranging from 40 to 70 mJ m^{-2} depending on the authors and the experimental techniques (Aulin et al., 2009; Erbil, 1996; Forsstroem et al., 2005; Mills et al., 2008; Swaminathan et al., 2006; Trejo-O'Reilly et al., 1998). These experimental values are indeed three to five times lower than our calculated ones, which range from 150 to 350 mJ m^{-2}, the lowest being for the hydrophobic (1 0 0)β and the highest for the hydrophilic (0 1 0)β surfaces. In fact, most of the experimental values result from inverse gas chromatography data on columns packed with specific cellulose substrates such as Avicell or Whatman paper (Mills et al., 2008; Swaminathan et al., 2006; Trejo-O'Reilly et al., 1998). Other data that essentially lead to similar surface energy values are deduced from contact angle measurements of liquid drops of various polarities on flat cellulose substrates (Aulin et al., 2009; Erbil, 1996; Forsstroem et al., 2005; Trejo-O'Reilly et al., 1998). As opposed to our calculations, which consider only infinite defect-free surfaces, these experimental measurements deal with complex substrates that expose not only a variety of perfect crystalline surfaces, but also a large number of voids, crystallite overlaps, etc. The occurrence of all these defects yields under-estimated surface energies. Thus, the calculated values that we are giving, correspond to upper limit of the surface energies. In our work, differentiation could be made between the various crystalline surfaces and in particular, we could show that the energy of the hydrophilic surface (0 1 0)β was more than twice that of the hydrophobic (1 0 0)β. So far, such differentiations cannot be made in experimental measurements, which consequentely yield only averaged data.

In this paper we have shown the differences that one can expect between the considered surfaces of cellulose. The question, which is raised, is to know whether these surfaces are indeed present or just hypothetical in cellulose. Most of the current experimental knowledge on the surfaces of cellulose crystals, results from the ultrastructural observations done on model cellulose systems such as those of *Valonia* or tunicin microfibrils or microcrystals. With these, it is firmly established that the hydrophilic (1 1 0)β and (1 −1 0)β surfaces are vastly dominant, but in the squarish section of the microfibrils, the observation of blunt corners (Fig. 1) also indicates that the minor surfaces (0 1 0)β and (1 0 0)β are surmised. The dominant hydrophilic character of the (1 1 0)β and (1 −1 0)β surfaces explains well why a surface derivatization is easily obtained by using reagents directed toward primary and/or secondary alcohols, namely chlorosilanes (Gousse, Chanzy, Cerrada, & Fleury, 2004), isocyanates (Trejo-O'Reilly, Cavaille, & Gandini, 1997), amines (Araki, Kuga, & Magoshi, 2002; Lasseuguette, 2008), TEMPO (Montanari, Roumani, Heux, & Vignon, 2005), etc. When achieved under mild conditions, such derivatizations are limited exclusively to the cellulose surfaces, leaving therefore intact the underlying crystalline core of the cellulose specimens. Regarding the minor (0 1 0)β and (1 0 0)β surfaces, there is no experimental evidence to prove the existence or the reactivity of the former, but the latter has been evidenced and its hydrophobic reactivity proven. Indeed, during the initial step of biodegradation of cellulose, the cellulases Cel6A and Cel7B from *Trichoderma reseei* adsorb strongly on cellulose thanks to their cellulose binding modules (CBM), which present three solvent-exposed aromatic amino acids: tyrosine in Cel6A or tryptophan in Cel7B (Lehtio et al., 2003). The cloning of these CBMs and their adsorption on opposite blunt corners of *Valonia* microcrystals and their identification by electron microdiffraction, has proven without ambiguity the existence of the minor (1 0 0)β surface and its attraction for hydrophobic reagents.

One may wonder why in large cellulose crystals such as those of *Valonia*, it is the fact that the (1 1 0)β and (1 −1 0)β surfaces are developed, and not the (1 0 0)β Indeed, there are two theories that predict external crystal shapes (Rohl, 2003): (i) the "equilibrium morphology" method is based on the surface energy: the surface of lowest surface energy dominates the morphology at thermodynamic equilibrium; (ii) the "growth morphology" method is based on the attachment energy: the attachment energy of a surface is proportional to its growth level and, thus, inversely proportional to its morphological importance. The (1 0 0)β surface has the smallest surface energy and the highest attachment energy; it should in principle dominate the external morphology. Despite the fact that the biosynthesis of cellulose crystals is not fully understood, the

current knowledge is that the microfibrils are produced by the so called "terminal complexes" (TCs) where the cellulose chains are first biosynthesized and then assembled and spun through the TC spinneret. These dynamics, being far from that of classical crystallization processes, must be responsible for the development of the (1 1 0)β and (1 −1 0)β surfaces. It has been proposed (Cousins & Brown, 1995) that during biosynthesis, the driving mechanism for the crystallization of the cellulose microfibril was not due to hydrogen bonding interactions, but rather to Van-der-Waals forces, associating the cellulose chains first into mini-sheets, then in mini-crystals and finally into microfibrils. This proposed mechanism would well explain the occurrence of the exposed (1 1 0)β surface and the presence of (1 0 0)β, but it fails to account for the (1 −1 0)β, which is as developed as the (1 1 0)β in the *Valonia* microfibril. Thus, it seems to us that at this stage, no clear explanation can account for the observed planes, which define the surface of cellulose microfibrils. One needs to wait for the full description of the mechanism of cellulose biosynthesis before giving a full explanation.

In this work, we have considered eight surfaces for cellulose crystals: four of them for the I-α and four for the I-β allomorphs. Among these, the existence of six of them has been proven in the case of the large crystal of *Valonia* cellulose, whereas two, namely the (1 1 0)α and (0 1 0)β have not been evidenced. Other surfaces of higher Miller indices may also be present in minor amount. In fact, the observation of microfibril sections, such as shown in Fig. 1, indicates that in several squarish microfibrils, there are one or two corners missing, exposing surfaces different from the dominant (0 1 0)α, (1 0 0)α and the (1 1 0)β and (1 −1 0)β. At present these minor surfaces have not yet been fully characterized and it could be that some of them are different from the minor (1 1 0)α, (1 −1 0)α, (0 1 0)β and (1 0 0)β that have been considered here.

Acknowledgements

The author thanks H. Chanzy for valuable discussions and comments during the writing of this work.

Fig. 1 was kindly provided by J.-F. Sassi. This work was funded by the Agence Nationale de la Recherche, ANR-08-BLAN-0009-03.

References

Araki, J., Kuga, S., & Magoshi, J. (2002). Influence of reagent addition on carbodiimide-mediated amidation for poly(ethylene glycol) grafting. *Journal of Applied Polymer Science*, *85*, 1349–1352.

Aulin, C., Ahola, S., Josefsson, P., Nishino, T., Hirose, Y., Oesterberg, M., et al. (2009). Nanoscale cellulose films with different crystallinities and mesostructures – Their surface properties and interaction with water. *Langmuir*, *25*, 7675–7685.

Baker, A. A., Helbert, W., Sugiyama, J., & Miles, M. J. (1998). Surface structure of native cellulose microcrystals by AFM. *Applied Physics A: Materials Science & Processing*, *A66*, S559–S563.

Baker, A. A., Helbert, W., Sugiyama, J., & Miles, M. J. (2000). New insight into cellulose structure by atomic force microscopy shows the Ialpha crystal phase at near-atomic resolution. *Biophysical Journal*, *79*, 1139–1145.

Bergenstrahle, M., Mazeau, K., & Berglund, L. (2008). Molecular modelling of interfaces between cellulose and surrounding molecules – Effects of caprolactone surface grafting. *European Polymer Journal*, *44*, 3662–3669.

Bergenstrahle, M., Wohlert, J., Larsson Per, T., Mazeau, K., & Berglund Lars, A. (2008). Dynamics of cellulose–water interfaces: NMR spin-lattice relaxation times calculated from atomistic computer simulations. *Journal of Physical Chemistry B*, *112*, 2590–2595.

Besombes, S., & Mazeau, K. (2005a). The cellulose/lignin assembly assessed by molecular modeling. Part 1: Adsorption of a threo guaiacyl beta-O-4 dimer onto a Ibeta cellulose whisker. *Plant Physiology and Biochemistry*, *43*, 299–308.

Besombes, S., & Mazeau, K. (2005b). The cellulose/lignin assembly assessed by molecular modeling. Part 2: Seeking for evidence of organization of lignin molecules at the interface with cellulose. *Plant Physiology and Biochemistry*, *43*, 277–286.

Biermann, O., Hadicke, E., Koltzenburg, S., & Muller-Plathe, F. (2001). Hydrophilicity and lipophilicity of cellulose crystal surfaces. *Angewandte Chemie: International Edition*, *40*, 3822–3825.

Carpita, N. C., & Gibeaut, D. M. (1993). Structural models of primary cell walls in flowering plants: Consistency of molecular structure with the physical properties of the walls during growth. *Plant Journal*, *3*, 1–30.

Chauve, G., Heux, L., Arouini, R., & Mazeau, K. (2005). Cellulose poly(ethylene-co-vinyl acetate) nanocomposites studied by molecular modeling and mechanical spectroscopy. *Biomacromolecules*, *6*, 2025–2031.

Cousins, S. K., & Brown, R. M., Jr. (1995). Cellulose I microfibril assembly: Computational molecular mechanics energy analysis favors bonding by van der Waals forces as the initial step in crystallization. *Polymer*, *36*, 3885–3888.

Da Silva Perez, D., Ruggiero, R., Morais, L. C., Machado, A. E. H., & Mazeau, K. (2004). Theoretical and experimental studies on the adsorption of aromatic compounds onto cellulose. *Langmuir*, *20*, 3151–3158.

Daele, Y. V., Revol, J.-F., Gaill, F., & Goffinet, G. (1992). Characterization and supramolecular architecture of the cellulose–protein fibrils in the tunic of the sea peach (*Halocynthia papillosa*, *Ascidiacea Urochordata*). *Biologie Cellulaire*, *76*, 87–96.

Donnay, J. D. H., & Harkei, D. (1937). A new law of crystal morphology extending the law of Bravais. *American Mineralogist*, *22*, 446–467.

Erbil, H. Y. (1996). Surface energetics of films of poly(vinyl acetate-butyl acrylate) emulsion copolymers. *Polymer*, *37*, 5483–5491.

Forsstroem, J., Eriksson, M., & Waagberg, L. (2005). A new technique for evaluating ink–cellulose interactions: Initial studies of the influence of surface energy and surface roughness. *Journal of Adhesion Science and Technology*, *19*, 783–798.

Gandini, A., & Belgacem, M. N. (2005). Modified cellulose fibers as reinforcing fillers for macromolecular matrices. *Macromolecular Symposium*, *221*, 257–270.

Gousse, C., Chanzy, H., Cerrada, M. L., & Fleury, E. (2004). Surface silylation of cellulose microfibrils: Preparation and rheological properties. *Polymer*, *45*, 1569–1575.

Hanley, S. J., Giasson, J., Revol, J. F., & Gray, D. G. (1992). Atomic force microscopy of cellulose microfibrils: Comparison with transmission electron microscopy. *Polymer*, *33*, 4639–4642.

Hanus, J., & Mazeau, K. (2006). The xyloglucan–cellulose assembly at the atomic scale. *Biopolymers*, *82*, 59–73.

Heiner, A. P., Kuutti, L., & Teleman, O. (1998). Comparison of the interface between water and four surfaces of native crystalline cellulose by molecular dynamics simulations. *Carbohydrate Research*, *306*, 205–220.

Heiner, A. P., & Teleman, O. (1997). Interface between monoclinic crystalline cellulose and water: Breakdown of the odd/even duplicity. *Langmuir*, *13*, 511–518.

Helbert, W., Nishiyama, Y., Okano, T., & Sugiyama, J. (1998). Molecular imaging of *Halocynthia papillosa* cellulose. *Journal of Structural Biology*, *124*, 42–50.

Helbert, W., Sugiyama, J., Kimura, S., & Itoh, T. (1998). High-resolution electron microscopy on ultrathin sections of cellulose microfibrils generated by glomerulocytes in *Polyzoa vesiculiphora*. *Protoplasma*, *203*, 84–90.

Himmel, M. E., Ding, S.-Y., Johnson, D. K., Adney, W. S., Nimlos, M. R., Brady, J. W., et al. (2007). Biomass recalcitrance: Engineering plants and enzymes for biofuels production. *Science*, *315*, 804–807.

Kim, N.-H., Herth, W., Vuong, R., & Chanzy, H. (1996). The cellulose system in the cell wall of Micrasterias. *Journal of Structural Biology*, *117*, 195–203.

Lasseuguette, E. (2008). Grafting onto microfibrils of native cellulose. *Cellulose (Dordrecht, The Netherlands)*, *15*, 571–580.

Lehtio, J., Sugiyama, J., Gustavsson, M., Fransson, L., Linder, M., & Teeri, T. T. (2003). The binding specificity and affinity determinants of family 1 and family 3 cellulose binding modules. *Proceedings of the National Academy of Sciences of the United States of America*, *100*, 484–489.

Mazeau, K. (2005). Structural micro-heterogeneities of crystalline Iβ-cellulose. *Cellulose*, *12*, 339–349.

Mazeau, K., & Heux, L. (2003). Molecular dynamics simulations of bulk native crystalline and amorphous structures of cellulose. *Journal of Physical Chemistry B*, *107*, 2394–2403.

Mazeau, K., & Rivet, A. (2008). Wetting the (1 1 0) and (1 0 0) surfaces of Ibeta cellulose studied by molecular dynamics. *Biomacromolecules*, *9*, 1352.

Mazeau, K., & Vergelati, C. (2002). Atomistic modeling of the adsorption of benzophenone onto cellulosic surfaces. *Langmuir*, *18*, 1919–1927.

Mills, R. H., Gardner, D. J., & Wimmer, R. (2008). Inverse gas chromatography for determining the dispersive surface free energy and acid-base interactions of sheet molding compound – Part II. 14 Ligno-cellulosic fiber types for possible composite reinforcement. *Journal of Applied Polymer Science*, *110*, 3880–3888.

Montanari, S., Roumani, M., Heux, L., & Vignon, M. R. (2005). Topochemistry of carboxylated cellulose nanocrystals resulting from TEMPO-mediated oxidation. *Macromolecules*, *38*, 1665–1671.

Newman, R. H., & Davidson, T. C. (2004). Molecular conformations at the cellulose–water interface. *Cellulose*, *11*, 23–32.

Nishiyama, Y. (2009). Structure and properties of the cellulose microfibril. *Journal of Wood Science*, *55*, 241–249.

Nishiyama, Y., Kim, U.-J., Kim, D.-Y., Katsumata, K. S., May, R. P., & Langan, P. (2003). Periodic disorder along ramie cellulose microfibrils. *Biomacromolecules*, *4*, 1013–1017.

Nishiyama, Y., Langan, P., & Chanzy, H. (2002). Crystal structure and hydrogen-bonding system in cellulose Iβ from synchrotron X-ray and neutron fiber diffraction. *Journal of the American Chemical Society*, *124*, 9074–9082.

Nishiyama, Y., Sugiyama, J., Chanzy, H., & Langan, P. (2003). Crystal structure and hydrogen bonding system in cellulose Iα from synchrotron X-ray and neutron fiber diffraction. *Journal of the American Chemical Society*, *125*, 14300–14306.

Nose, S. (1984a). A molecular dynamics method for simulations in the canonical ensemble. *Molecular Physics*, *52*, 255–268.

Nose, S. (1984b). A unified formulation of the constant temperature molecular dynamics methods. *Journal of Chemical Physics*, *81*, 255–268.

Rappe, A. K., & Goddard, W. A. (1991). Charge equilibration for molecular dynamics simulations. *Journal of Physical Chemistry*, *95*, 3358–3363.

Revol, J. F. (1982). On the cross-sectional shape of cellulose crystallites in *Valonia ventricosa*. *Carbohydrate Polymers*, *2*, 123–134.
Rohl, A. L. (2003). Computer prediction of crystal morphology. *Current Opinion in Solid State and Materials Science*, *7*, 21–26.
Sassi, J.-F., & Chanzy, H. (1995). Ultrastructural aspects of the acetylation of cellulose. *Cellulose*, *2*, 111–127.
Sassi, J.-F., Tekely, P., & Chanzy, H. (2000). Relative susceptibility of the Iα and Iβ phases of cellulose towards acetylation. *Cellulose*, *7*, 119–132.
Sugiyama, J., Harada, H., Fujiyoshi, Y., & Uyeda, N. (1985). Lattice images from ultrathin sections of cellulose microfibrils in the cell wall of *Valonia macophysa* kutz. *Planta*, *166*, 161–168.
Sugiyama, J., Vuong, R., & Chanzy, H. (1991). Electron diffraction study on the two crystalline phases occurring in native cellulose from an algal cell wall. *Macromolecules*, *24*, 4168–4175.
Sun, H., Mumby, S. J., Maple, J. R., & Hagler, A. T. (1994). An ab initio CFF93 all atom force fields for polycarbonates. *Journal of the American Chemical Society*, *116*, 2978–2987.
Swaminathan, V., Cobb, J., & Saracovan, I. (2006). Measurement of the surface energy of lubricated pharmaceutical powders by inverse gas chromatography. *International Journal of Pharmaceutics*, *312*, 158–165.
Trejo-O'Reilly, J.-A., Cavaille, J.-Y., Belgacem, N. M., & Gandini, A. (1998). Surface energy and wettability of modified cellulosic fibers for use in composite materials. *Journal of Adhesion*, *67*, 359–374.
Trejo-O'Reilly, J.-A., Cavaille, J.-Y., & Gandini, A. (1997). The surface chemical modification of cellulosic fibers in view of their use in composite materials. *Cellulose*, *4*, 305–320.
Tvaroska, I., & Carver, J. P. (1997). Ab initio molecular orbital calculation of carbohydrate model compounds 6. The gauche effect and conformations of the hydroxymethyl and methoxymethyl groups. *Journal of Physical Chemistry B*, *101*, 2992–2999.
Verlet, L. (1967). Computer experiments on classical fluids I. Thermodynamical properties of Lennard-Jones molecules. *Physical Review*, *159*, 98–103.
Vietor, R. J., Newman, R. H., Ha, M.-A., Apperley, D. C., & Jarvis, M. C. (2002). Conformational features of crystal-surface cellulose from higher plants. *Plant Journal*, *30*, 721–731.
Xu, Q., Tucker, M. P., Arenkiel, P., Ai, X., Rumbles, G., Sugiyama, J., et al. (2009). Labeling the planar face of crystalline cellulose using quantum dots directed by type-I carbohydrate-binding modules. *Cellulose*, *16*, 19–26.